焊条典型熔滴过渡形态的判读

王 宝[1]， 杨 林[1]， 王 勇[2]
（1. 中北大学 焊接材料技术中心，太原 030051；
2. 太原理工大学 焊接材料研究所，太原 030024）

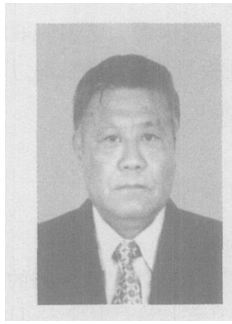

王 宝

摘 要：粗熔滴短路过渡，渣壁过渡，爆炸过渡和喷射过渡是焊条的基本过渡形态。过去一直采用光电示波器记录的电弧电压、焊接电流波形图，定性地描述熔滴过渡的一般特征，不可能进行精确的定量分析。通过对汉诺威弧焊质量分析仪获取的焊条四种典型熔滴过渡形态的电弧电压、焊接电流概率密度分布图的特征和短路时间 t_1、燃弧时间 t_2、加权燃弧时间 t_3 和过渡周期 t_C 的数据进行统计分析，可精确地描述焊条熔滴过渡形态的电弧物理特征，并能够判别焊条熔滴过渡形态。为焊条熔滴过渡形态的判定提供了一种新方法。

关键词：焊条；焊接电弧物理；熔滴过渡；汉诺威弧焊质量分析仪
中图分类号：TG 422.3 文献标识码：A 文章编号：0253－360X(2006)11－095－04

0 序 言

焊条电弧焊时焊条熔滴过渡形态对焊条工艺性有直接的关系，焊条熔滴过渡形态的判别对研究评价焊条的工艺性至关重要。电弧焊接过程是一个随机过程，在任何一个瞬间电弧电压、焊接电流都在发生变化，过去一直采用示波器记录的波形图来描述这一随机过程。这种波形图虽然可以对焊接过程电参数进行直观形象的描述，也可以对过渡频率、过渡周期等熔滴过渡现象定性的粗略分析，但是它不可能进行精确的定量分析和评定。

近年来德国汉诺威大学“材料连接焊接工艺研究中心”开发了以现代计算机技术为基础的汉诺威弧焊质量分析仪，为焊接电参数的测试提供了新手段，使焊条或焊丝过渡形态特征的科学描述和对其工艺性能的科学评价成为可能。作者采用汉诺威弧焊质量分析仪对焊条电弧焊的熔滴过渡形态进行分析，并探讨焊条熔滴过渡形态判别的新方法。

1 试验仪器及试验条件

1.1 汉诺威弧焊质量分析仪

汉诺威弧焊质量分析仪能够对焊接过程电弧电压和焊接电流信号大量的取点，准确描述电弧电压和焊接电流的随机变化，显示电压和电流的概率密度分布，记录短路时间、燃烧时间、短路周期等参数，并进行精确的数据统计和文件编制[1,2]，是当今弧焊电参数研究的重要工具。

1.2 熔滴过渡过程的高速摄影

高速摄影技术是研究熔滴行为的不可替代的手段，作者采用德国产 Pentazet－16 型和国产 LSB－16 型高速摄影机，以 1000－2000f/s 摄影速度研究焊接过程中熔滴行为，获取熔滴行为的丰富信息。

1.3 试验焊条样品的选取

试验选取四种典型过渡形态的焊条，钛钙型不锈钢焊条是典型粗熔滴过渡形态的焊条，该焊条是为了试验目的由太原理工大学焊接材料研究所专门压制的，试验焊条编号为 TY102－B（规格为 ϕ4.0 mm）；钛型不锈钢焊条作为渣壁过渡形态的试验焊条，焊条编号为E308－12（规格为 ϕ3.2 mm）；钛钙型结构钢焊条具有多种熔滴过渡形态共存的特点，有明显的熔滴爆炸过渡的成分，选择其作为爆炸过渡形态的样品焊条，编号为 E4303－01（规格为 ϕ3.2 mm）；EDP－A2－03 型堆焊焊条，由于药皮中存在多量的高碳铁合金，同时设计为氧化性强的钛钙型药皮，熔滴为典型的喷射过渡形态，试验焊条编号为 TYD132（规格为 ϕ4.0 mm）。

1.4 试验条件

试验所采用的实际焊接参数见表 1。

收稿日期：2006－02－10

表 1 实际焊接电参数

Table 1 Electricity parameters on actual welding

试验焊条编号	TY102—B	E308—12	E4303—01	TYD132
焊接电流 I/A	136.15	119.01	112.88	132.31
电弧电压 U/V	21.11	30.52	22.96	26.46

焊接电源为 ZXG—300 型弧焊整流器，直流反接试板材料为 Q235 钢，尺寸 250 mm× 50 mm× 8 mm。

2 试验结果

2.1 焊条熔滴过渡形态的一般特征

焊条熔滴过渡形态可以分为粗熔滴过渡，渣壁过渡，爆炸过渡和喷射过渡四种类型。这几种过渡形态的特征，在文献[3]中已作了详细地分析，这里选取有代表性的高速摄影照片[4]，对焊条熔滴过渡的特征加以概括地描述。

图 1 是一组焊条四种典型熔滴短路过渡高速摄影照片，图 1a，b，c 是粗熔滴过渡的画面，图 1a 是大熔滴悬挂在焊条端部的情形，看出熔滴尺寸很大，接近甚至于超过焊芯的直径，由于熔滴粗大，熔滴过渡时与熔池发生短路，并时常引起电爆炸飞溅。从图 1b可以看出，熔滴与熔池之间形成了短路桥，接着短路桥发生了爆炸，引起强烈的电爆炸飞溅（图 1c），这种爆炸飞溅对焊条工艺性影响很大。

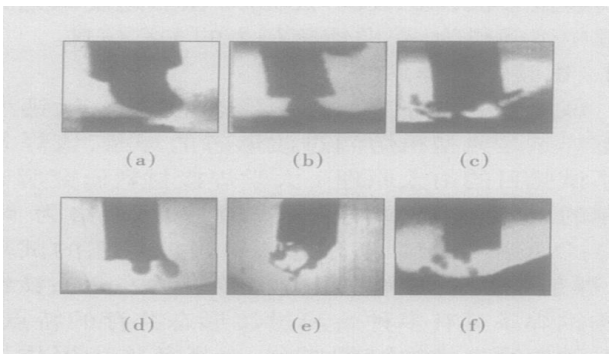

图 1 焊条四种过渡形态的高速摄影照片

Fig. 1 High speed photograph of four kinds of typical transfer modes for the covered electrodes

渣壁过渡是熔滴沿着焊条套筒的壁面滑向熔池的一种过渡形式，见图 1d，它的主要特征是，熔滴尺寸小，在焊条端部有时同时存在着两个以上的熔滴，由于熔滴过渡时一般不与熔池发生短路，因此一般不会发生猛烈的电爆炸飞溅，经常出现的只是飘落的飞溅，对焊条工艺性影响不很大。熔滴过渡频率一般 7 ~ 9 s^{-1}，比短路过渡时要大一些。焊条熔滴为渣壁过渡时电弧稳定，飞溅小，熔化效率高，综合工艺性最好，是一种理想的熔滴过渡形式。

图 1e 是熔滴发生爆炸过渡时的高速摄影的照片。所谓爆炸过渡是指熔滴在形成、长大或过渡过程中，由于激烈的冶金反应，在熔滴内部产生 CO 气体，使较大的熔滴急剧膨胀发生爆炸而形成的一种过渡形式。爆炸过渡破坏了电弧稳定性，带来的强烈爆炸飞溅，严重恶化了焊接工艺性。熔滴爆炸过渡的频率大约为 30 ~ 50 s^{-1}。

图 1f 是焊条熔滴发生喷射过渡时的高速摄影照片。可以看出焊条端部熔体呈细碎的颗粒由套筒内喷射出来，并以喷射状态快速通过电弧空间向熔池过渡，熔滴细碎程度比爆炸过渡时要大得多。过渡频率一般超过 100 s^{-1}。喷射过渡时虽然电弧稳定，但它形成过于强烈的喷洒飞溅明显地恶化了焊条工艺性。

2.2 汉诺威弧焊质量分析仪对典型焊条的测试

2.2.1 典型焊条电弧电压概率密度分布

图 2 是用汉诺威弧焊质量分析仪测试得到的四种典型过渡形态焊条的电弧电压概率密度分布叠加图。横坐标为电弧电压，纵坐标是以对数形式表示的焊接过程电弧电压的概率。

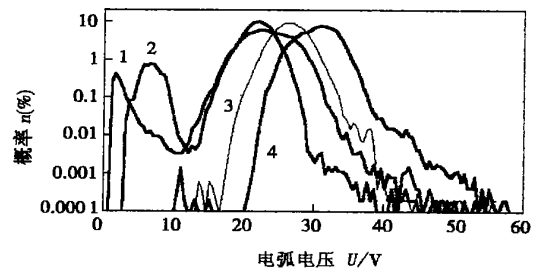

图 2 焊条四种典型熔滴过渡形态电压概率密度分布叠加图

Fig. 2 Probability density distributions of arc voltage of four kinds of typical transfer modes for covered electrodes

2.2.2 典型焊条焊接电流概率密度分布

用汉诺威焊接质量分析仪测试的焊接电流概率密度分布叠加曲线见图 3。横坐标为焊接电流，纵坐标是以对数形式表示的焊接过程电流的概率。

图 2 和图 3 中曲线 1（焊条名称 TY102—B）为粗熔滴短路过渡，曲线 3（焊条名称 E308—12）为渣壁

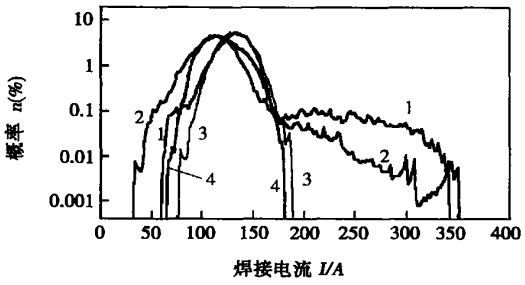

图 3　焊条四种典型过渡形态电流概率密度分布叠加图

Fig. 3　Probability density distributions of welding currents of four kinds of typical transfer modes for covered electrodes

过渡,曲线 2 (焊条名称 E4303—01) 为爆炸过渡,曲线 4(焊条名称 TYD132)为喷射过渡。

2.2.3　典型焊条的 t_1, t_2, t_3 和 t_c 的测试结果

测试的四种焊条的短路时间 t_1, 燃弧时间 t_2, 加权燃弧时间 t_3 和周期时间 t_C 的数据见表 2。表中还列出了在测试的时间内焊条发生短路的概率之和$\sum n(U_s)$、短路大电流概率之和$\sum n(I_s)$、短路频率 f 和电压变异系数 $s(U)$的测试结果。

由于渣壁过渡和喷射过渡时熔滴不与熔池短路, 所以 E308—12 和 TYD132 焊条 t_1, t_2, t_3 和 t_c 没有数据, 也不会出现$\sum n(U_s)$, $\sum n(I_s)$, f 和变异系数 $s(U)$的数据。

表 2　焊条四种典型过渡形态的测试数据

Table 2　Testing data for four kinds typical transfer modes for covered electrodes

试验焊条名称	电弧电压 U/V	焊接电流 I/A	变异系数 $s(U)$%	电压概率和 $\sum n(U_s)n$(%)	电流概率和 $\sum n(I_s)n$(%)	短路频率 f/s^{-1}	短路时间 t_1/μs	燃弧时间 t_2/μs	加权燃弧时间 t_3/μs	周期时间 t_c/μs
TY102—B	21.11	136.15	18.61	5.256 2	1.304 2	7.4	7 085.14	26 350.00	18 750.00	24 477.27
E308—12	30.50	119.01	8.66	—	—	—	—	—	—	—
E4303—01	22.96	112.88	17.17	1.531 8	0.297 6	16.8	1 039.19	24 802.63	40 892.86	43 392.86.
TYD132	26.46	132.31	8.44	—	—	—	—	—	—	—

3　试验结果的分析

3.1　焊条典型过渡形态的电弧电压概率密度分布图分析

图 2 中曲线 1(TY102—B 焊条)是典型的熔滴短路过渡形态的电压概率密度分布曲线, 可以看到它的主要特点是, 曲线为双驼峰状, 中部的高峰反映的是正常焊接过程的电弧电压的概率密度分布, 而图左面小驼峰对应的低电压的部分, 反映的是熔滴的短路行为形成的电压概率密度分布。熔滴越粗大, 短路时间越长, 短路形成的低电压概率越大, 小驼峰覆盖的电压范围越大。

由于熔滴的爆炸过渡形态也有短路过程发生, 所以具有爆炸过渡的 E4303—01 试验焊条的电压概率密度分布曲线 2 也具有双驼峰的特点。但是由于熔滴比前者细, 短路出现的概率也小, 因而小驼峰曲线也低一些, 它所覆盖的电压范围也小。由表 1 看出, 统计得到的爆炸过渡的 E4303—01 焊条短路概率和$\sum n(U_s)$数值很小, 仅为 1.531 8%, 而短路过渡的 TY102—B 焊条$\sum n(U_s)$为 5.256 2%, 比前者大得多。

显然具有渣壁过渡形态的钛型不锈钢焊条(图中曲线 3 焊条名称 E308—12), 它的电压概率密度分布曲线不存在小驼峰。由于渣壁过渡的焊条一般都会出现偶然的短路现象, 因此在电压概率密度分布图中左面低电压段有时也会出现低落的波动曲线。由于渣壁过渡焊条名义电压较高, 因此曲线在整体上比喷射过渡的曲线靠右。

TYD132 焊条为喷射过渡形态, 由于熔滴十分细小, 熔滴过渡行为对焊接电参数几乎没有影响, 电压概率密度分布曲线不仅不会出现小驼峰, 而且曲线覆盖的电压范围比任何过渡形态的曲线都窄(图 2 中曲线 4)。

3.2　焊条典型过渡形态的焊接电流概率密度分布图分析

由图 3 看出, 具有粗熔滴过渡的 TY102—B 焊条和爆炸过渡的 E4303—01 焊条焊接电流概率密度分布曲线是分散的, 由于这两种焊条熔滴都有短路过渡, 在熔滴短路时形成大的短路电流, 而在每个熔滴短路过渡完成后, 在电弧重燃的初期, 电流很小, 于是在图的右侧既有反映短路大电流的概率分布, 又有在图的左侧反映电弧重燃初期小电流的概率密度分布, 因此这两种焊条的焊接电流概率密度分布曲线比较分散。还可以看出图右侧表示的熔滴短路大电流的概率曲线, 粗熔滴过渡的 TY102—B 焊条(曲线 1)比爆炸过渡的 E4303—01 焊条(曲线 2)位置更靠上。统计的 TY102—B 和 E4303—01 焊条短路大电流(平均电流 2 倍)的概率和$\sum n(I_s)$分别为 1.304 2%, 和 0.297 6%, 这说明粗熔滴过渡的 TY102—B 焊条比爆炸过渡的 E4303—01 焊条短路

大电流出现的概率更大。

渣壁过渡的 E308—12 焊条和喷射过渡的 TYD132 焊条熔滴都不存在短路过渡，当然不会出现熔滴短路过渡引起的大电流和电弧重燃时形成的小电流，电流概率密度分布曲线比较收敛。很容易理解细熔滴的喷射过渡电流概率密度分布曲线相对更集中。

3.3 焊条典型过渡形态焊接相关参数的分析

由表 2 中四种典型过渡形态焊条平均短路时间 t_1、平均燃弧时间 t_2、平均加权燃弧时间 t_3（即忽略瞬时短路后统计的燃弧时间）和平均过渡周期 t_c 的数据看出，粗熔滴短路过渡的 TY102—B 焊条平均短路时间 t_1、平均燃弧时间 t_2 较长，这显然是因为 TY102—B 焊条熔滴粗大，熔滴长大所需要的时间长，同样熔滴短路的持续时间（向熔池过渡所需要的时间）也长。显然爆炸过渡的情况与前者不同，熔滴尺寸比较小，平均短路时间 t_1、平均燃弧时间 t_2 都小一些。熔滴为爆炸过渡的 E4303—01 焊条，由于熔滴的强烈运动形成的频繁的瞬间短路，使统计的平均燃弧时间 t_2 比 TY102—B 焊条短一些，而当忽略这一瞬间短路行为，统计的 E4303—01 焊条的加权燃弧时间 t_3 和过渡周期 t_c 明显地增大了。

4 基于汉诺威分析系统的焊条熔滴过渡形态的判别

将上述分析的焊条四种典型过渡形态的电弧电压、焊接电流概率密度分布图和平均电弧电压 U、焊接平均电流 I、平均短路时间 t_1、平均燃弧时间 t_2、加权燃弧时间 t_3、周期时间 t_c、短路电压概率之和 $\sum n(U_s)$、短路大电流概率和 $\sum n(I_s)$、短路频率 f 以及电压变异系数 $s(U)$ 等相关参数的基本特征可以归结为以下诸点。

① 渣壁过渡形态的平均电弧电压最高，而焊接平均电流最小。

② 粗熔滴短路过渡 t_1，t_2 比爆炸过渡时长，而 t_3 和 t_c 则相反，比爆炸过渡时短。

③ 粗熔滴过渡 $\sum n(U_s)$，$\sum n(I_s)$ 比爆炸过渡大。

④ 爆炸过渡短路频次 f 比粗熔滴过渡时高。

⑤ 渣壁过渡和喷射过渡形态 t_1，t_2，t_3，t_c，$\sum n(U_s)$，$\sum n(I_s)$ 以及 f 等相关参数趋于零。

根据以上特征可以分析和判别焊条基本过渡形态。

5 结 论

（1）粗熔滴短路过渡，渣壁过渡，爆炸过渡和喷射过渡是焊条的基本过渡形态。采用汉诺威弧焊质量分析仪能够对焊接过程电弧电压和焊接电流的随机变化进行快速精确统计，提供焊接过程电参数的大量信息，能对焊条过渡形态特征进行科学分析和描述。

（2）粗熔滴短路过渡和爆炸过渡电压概率密度分布图曲线均为双驼峰状，曲线右侧存在着高电压概率分布。粗熔滴短路过渡小驼峰曲线表示的短路电压概率和 $\sum n(U_s)$ 比爆炸过渡大。渣壁过渡和喷射过渡形态焊条的电压概率密度分布曲线不存在小驼峰。

（3）焊条粗熔滴过渡和爆炸过渡形态电流概率密度分布图均存在短路大电流概率分布，粗熔滴过渡比爆炸过渡的焊条短路大电流出现的概率更大。渣壁过渡和喷射过渡电流概率密度分布曲线比较集中。

（4）通过对焊条四种典型熔滴过渡形态相关参数 t_1，t_2，t_3，t_c，f，$\sum n(U_s)$，$\sum n(I_s)$ 和 $s(U)$ 特征的分析，可以判别焊条熔滴过渡形态的类型，为焊条熔滴过渡形态的判定提供了新方法。

参考文献：

[1] Rehfeldt D，Bollmann A. Using statistical signal analysis for analyzing and monitoring GMAW processes [A]. Proceedings of the Symposium on "Strategy of Welding Research in 2000 and Possible Aspects of China—Germany Cooperation"[C]. Beijing：China，1991.

[2] Rehfeldt D. Computer-aided quality assurance (CAQ) of Al—MIG welding with analysator Hannover[A]. 2003 汽车焊接国际论坛论文集[C]. 北京：机械工业出版社，2003.

[3] 王 宝. 焊接电弧物理与焊条工艺性设计[M]. 北京：机械工业出版社，1998.

[4] 王 宝. 焊接电弧物理与焊条设计的应用（光盘版）[M]. 北京：机械工业出版社，2003.

作者简介：王 宝，男，1937 年 6 月出生。教授。主要从事焊接冶金、焊接电弧物理及焊接材料方面的研究，取得 20 余项研究成果。获国家科技进步二等奖 1 项、部、省科技成果奖 10 余项，获得国家发明专利 5 项。出版两部专著，发表论文 40 余篇。

Email：wang9142t@163.com.

Technology, Beijing 100022, China). p77—80

Abstract: The effects of different shielding gases CO_2, Ar and mixture gases (CO_2 + Ar) on the slag detachability of type 347L flux-cored wire for stainless steels containing Nb were investigated. Slag detachability of home-made GDQA347L (3 #) was compared with that of TFW-347L flux-cored wire and AT-Y347L flux-cored in the same condition. The effects of slag microstructure and macroscop on the slag detachability of three type flux-cored wires were investigated. The results showed that the best slag detachability of GDQA347L flux-cored wire was under the shielding gas of Ar; and the better slag detachability was under the shielding gas of mixture gas (CO_2 + Ar), and the worst slag detachability was under the shielding gas of CO_2. Because the CO_2 gas transfer into active gas at high temperature with strong oxidizability which will make detachment difficult on the slag detachability, and it is proved that the regular of microstructure of three flux-cored wires under different shielding gases is similar. It is benefit for the slag detachability when the trunk of the strip-shaped slag microstructure is long and the area of the branch is large.

Key words: type 347L flux-cored wire for stainless steels; slag detachability; shielding gas

Auto-adapting heat source model for numerical analysis of friction stir welding LI Hong-ke, SHI Qing-yu, ZHAO Hai-yan, LI Ting (Department of Mechanical Engineering, Tsinghua University, Key Laboratory for Advanced Materials Processing Technology, Ministry of Education, Beijing 100084, China). p81—85

Abstract: The heat generation mechanism and dependency of material properties on temperature can't be fully characterized by the heat source models used now. According to friction mechanics, a heat generation model based on yield strength was established. The model can make auto-adaptation to material property and temperature variation and represent the physical nature during FSW process. Comparison between experiment of thermal field and simulation results indicates that the accuracy is quite good for this new heat model.

Key words: friction stir welding; temperature field; heat source model; numerical simulation

Effect of electromagnetic stirring on microstructure and properties of surfacing metal CHENG Jiang-bo[1,2], XU Bin-shi[2], LIU Zheng-jun[3], WU Yi-xiong[1] (1. School of Material Science and Engineering, Shanghai Jiaotong University, Shanghai 200240, China; 2. RM of the Academy of Armored Forces Engineering, Beijing 100072, China; 3. School of Material Science and Engineering, Shenyang University of Technology, Shenyang 110023, China). p86—90

Abstract: The effect of electromagnetic stirring on the microstructure and properties of surfacing metal during the applied longitudinal intermittent alternative magnetic field on low carbon steel with plasma arc surfacing are investigated and discussed. The surfacing metal was analyzed using optical metallography, X-ray diffraction, microhardness testing and wet sand rubber wheel abrasion testing. It's found that the hard phases are increasing and distributing homogeneously in the surface of surfacing layer with changing magnetic parameters and the wear resistance of surfacing metal is increasing gradually. The optimal result is acquired when the magnetic parameters are 3 A, 10 Hz. The experimental results indicate that the optimal effect of grain refining can be gained with the proper magnetic parameters and electromagnetic stirring can control the morphology of hard phase in surfacing metal. The morphology of hard phases with strip and hexagon distribution without magnetic field are shifted to only hexagon alignment distribution with proper magnetic field, which it can improve the hardness and wear resistance of surfacing metal greatly.

Key words: electromagnetic stirring; plasma arc surfacing; longitudinal magnetic field

Fracture toughness tests of D406A steel welded joints ZOU Ji-quan[1,2], JING Hong-yang[1], HUO Li-xing[1] (1. School of Material Science & Engineering, Tianjin University, Tianjin 300072, China; 2. School of Electromechanical and Automation, Tianjin Professional College, Tianjin 300402, China). p91—94

Abstract: In accordance with the fracture toughness test standard of BS7448, *J-R* curve tests were conducted with multiple specimen with welded joints of D406A ultra-high strength steel. According to the standard, the specimen with prefabricated fatigue crack has a standard 3 points bending shape that has a rectangular section of $B \times 2B$ (B: specimen thickness) and notch orientation of thickness direction. The load and load-line displacement of weld and heat affected zone were tested, and the values of J integral were calculated. Finally, *J-R* curves and the critical value of J were obtained through the data points best fitted. Thus the problem of failure to test the critical stress intensity factor in welded joints directly by lack of thickness of specimen was coped with and the reliable evidence was offered for the design of solid propellant rocket engine.

Key words: ultra-high strength steel; welded joint; J integral; resistance curve

Evaluation of typical metal transfer modes for covered electrode WANG Bao[1,2], YANG Lin[1], WANG Yong[2] (1. Technology Center for Welding Consumables, North University of China, Taiyuan 030051, China; 2. Institute of Welding Materials, Taiyuan University of Technology, Taiyuan 030024, China). p95—98

Abstract: There are four basic metal transfer modes, globular droplet transfer, flux-wall guided transfer, explosive transfer and spray transfer for covered electrode. Photoelectrical oscillograph is traditionally employed to analyze arc voltage and welding current as two major electric parameters for the purpose of understanding the stability degree of a welding operation. Only the general characteristic of metal transfer can be qualitatively described and the quantitative analysis can't be carried out. Those parameters, such as probability density distributions of arc voltage, welding current and the da-

ta of short-circuiting time t_1, burning time t_2, weighted burning time t_3, cycle time t_c, which are existed in four kinds of typical metal transfer modes and can be added up and analyzed by ANALYSATOR HANNOVER. Four typical metal transfer modes can be evaluated by analyzing above-mentioned parameters. The arc physical characteristic of different metal transfer modes can be accurately described. The statistical analysis of electric parameters, which are collected by ANALYSATOR HANNOVER, provide a new method to determine the metal transfer mode for the covered electrodes.

Key words: covered electrode; welding arc physics; metal transfer; ANALYSATOR HANNOVER

Vacuum hot roll bonding of titaium to stainless steel using Cu and Nb composite interlayer ZHAO Dong-sheng, YAN Jiu-chun, WANG Yong, YANG Shi-qing (State Key Laboratory of Advanced Welding Production Technology, Harbin Institute of Technology, Harbin 150001, China). p99—102

Abstract: This article describes a study of the application of a vacuum hot roll bonding technique to Ti alloy plate and stainless steel plate using the composite interlayer of copper (pure copper and copper contains lanthanon Yt) and Nb sheet. The tensile strength was tested and the microstructure of the joint interface, fractograph and the structure of copper interlayer were analyzed by optical and scanning electron microscopy, XRD, energy spectrum analysis. The results showed that the defects such as separation and crack were not observed at interface, and there are no intermetallic compounds formed after bonding. There existed a transition layer at Nb-Ti interface, the thickness of which is about 2.5 μm and the thickness of transition layer at Cu-SS and Nb-Cu interface is about 1.9 μm. At copper grain boundary the voids were observed and the fractograph showed crack along the grain boundary. Doping of the lanthanon Yt can reduce the grain size. No voids appear in copper layer with Yt comparing with without Yt with the same bonding parameters, and the effect of reducing grain size is more efficient with the content of Yt in copper increasing from 0.01% to 0.02wt%. Comparing with the specimen using pure copper interlayer, the tensile strength increased 51.3 MPa (Yt 0.01wt% in Cu) and 61.7 MPa (Yt 0.02wt% in Cu), respectively.

Key words: vacuum hot roll bonding; Ti alloy; stainless steel

Pitting resistant test of welded joint of YUS270 steel DUAN Yang-zhong, ZHANG Yu-feng, HUO Li-xing (School of Material Science & Engineering, Tianjin University, Tianjin 300072, China). p103—105

Abstract: YUS270 steel is a super austenitic stainless steel produced by Japan and has a perfect pitting resistance. The specimens had been put into the hydrochloric acid with $FeCl_3$ for testing pitting resistance. The experiment was based on ASTM G-48 Test Method C at 40 ℃. Then the losing weight, pitting density and maximal depth were compared. The results showed that all the items satisfied the standard in this condition. It also proved the excellent pitting resistance of Cl^{-1} of YUS270 steel and provided the evidence for the application in the offshore oil platform.

Key words: YUS270 steel; super austenitic stainless steel; pitting

Forming mechanism of flash butting welded joint of SiC particle reinforced aluminium matrix composite (SiC_p/3003Al) TU Yi-min, LI Xing-rui (Material Science and Engineering College, Henan University of Science and technologe, Luoyang 471003, Henan, China). p106—108

Abstract: The studies were conducted by flash butting welding of SiC particle reinforced 3003 aluminium matrix composites. The welding process of SiC particle reinforced 3003 aluminium matrix composite can be conducted effectively and the joint of high quality can be gained under the appropriate flash butting welding parameters. The forming mechanism of the joint was studied by means of EDX unit and SEM. The distribution of SiC particles in the joint and interface reaction of SiC-Al were analyzed and discussed. The results show that the impurities of gas and solid state can be removed and the sound joint without gas hole, impurities and cracking can be gained by means of the burst of metal beam and the plastic deformation of joint interface in the flash butting welding process, and the joint possesses high strength owing to the SiC particle gathering in the joint zone. When the SiC-Al reacted, the harmful affection for the joint quality can be reduced because of low welding temperature and short welding time in the flash butting welding process.

Key words: metallic matrix composite; flash butting welding; welded joint

Three dimensional finite element numerical simulation of temperature and stress in modest hot slide FENG Ming-jie[1], WU Hai-xia[2] (1. Key Laboratory for Electromagnetic Processing of Materials of Ministry of Education, Northeastern University, Shenyang 110004, China; 2. Anyang Iron &Steel Ltd. Co., Anyang 455004, Henan, China). p109—112

Abstract: On the base of the thermal-elastic theory, the three-dimensional finite element numerical analysis simulated distribution of temperature, strain and stress in the modest hot slides with ANSYS sequential coupling analyzing heat transfer and stress equations. The results show that the highest temperature rises with increasing of height of the slide and reduces with increasing of length of the slide, and the highest temperature of trapezoid slide is lower 15—20 ℃ than that of rectangle slide at the same time. The highest equivalent stress for the rectangle slide is bigger than that of the trapezoid slide at the same time, and it lies in weld and rises with increasing height and length of the slide.

Key words: heating furnace; modest hot slide; temperature distribution; stress distribution